J. Inst. Eng. India Ser. B (August 2021) 102(4):807–818
https://doi.org/10.1007/s40031-021-00571-z

ORIGINAL CONTRIBUTION

Probabilistic Principal Component Analysis and Long Short-Term Memory Classifier for Automatic Detection of Alzheimer's Disease using MRI Brain Images

Halebeedu Subbaraya Suresha[1] · **Srirangapatna Sampathkumaran Parthasarathy**[2]

Received: 14 September 2020 / Accepted: 2 March 2021 / Published online: 20 March 2021

Abstract Automatic detection of Alzheimer's disease using magnetic resonance imaging is a hard task, due to the complexity and variability of the size, location, texture, and shape of the lesions. The objective of this study is to propose a proper feature dimensional reduction and classifier to improve the performance of Alzheimer's disease detection. At first, the brain images are acquired from Open Access Series of Imaging Studies and National Institute of Mental Health and Neuro Sciences databases. Then, contrast-limited adaptive histogram equalization and normalization technique are applied for improving the visual ability of the collected raw images. Next, discrete wavelet transform is used to transform the denoised images in order to extract the feature vectors, and probabilistic principal component analysis algorithm is developed to decrease the dimension of the extracted features that effectively lessen the "curse of dimensionality" concern. At last, long short-term memory classifier is used for classifying the brain images as Alzheimer's disease, normal, and mild cognitive impairment. From the simulation result, the proposed system obtained better performance compared with the existing systems and showed 3–11% improvement in recognition accuracy.

Keywords Alzheimer's disease · Discrete wavelet transform · Long short term memory · Normalization · Probabilistic principal component analysis

✉ Halebeedu Subbaraya Suresha
srisuri75@gmail.com

[1] Department of ECE, PET Research Centre, Mandya, University of Mysore, Mysore, India

[2] Department of ECE, P.E.S College of Engineering, Mandya, India

Introduction

Alzheimer's disease is a degenerative brain disorder, which leads to memory loss, poor language or problem solving and thinking, that extremely affects the individual's daily life [1, 2]. Presently, the neuroimaging techniques are extensively used in Alzheimer's disease recognition and classification that delivers a way for physicians to investigate the functional and structural changes in the brain [3, 4]. The most commonly used imaging modalities in Alzheimer's disease recognition are magnetic resonance imaging (MRI), functional MRI, positron emission tomography, diffusion tensor imaging, etc. [5, 6]. Among the available imaging modalities, MRI scan gains more attention among the researchers, because of its easy access in the clinical settings, and the functional and structural changes in the brain related to Alzheimer's disease are non-invasively evaluated [7–9]. However, the manual analysis of Alzheimer's disease by the clinicians may not be accurate and consumes more time for detection [10]. So, the automatic recognition of Alzheimer's disease has made an impression in the research community [11, 12]. In recent decades, several methods are developed by the researchers for Alzheimer's disease detection [13–15].

T. Altaf et al. [16] developed a new automated system for Alzheimer's disease detection and classification. In this literature, the texture feature descriptors like histogram of gradient, gray level co-occurrence matrix, local binary pattern, and scale invariant feature transform were applied for extracting the features from the brain images.

Further, the classification phase was validated with dissimilar approaches like decision tree, k-nearest neighbor (KNN), support vector machine (SVM), and ensemble classifiers in order to classify the images as three classes; normal, MCI, and Alzheimer's disease. Still, the semantic

space between the extracted texture features was very high that leads to poor classification of the images. D. Jha et al. [17] presented a supervised system for Alzheimer's disease recognition on the basis of PCA, feed forward neural network (FNN), and dual tree complex wavelet transform (DTCWT). However, FNN classifier was related to an application domain, so it was limited to static concerns due to its feed forward structure. D. Jha et al. [18] developed a system for Alzheimer's disease detection on the basis of DTCWT, PCA, linear discriminant analysis (LDA), and ensemble classifier. In this literature, the DTCWT method was utilized for extracting the feature vectors from the acquired images. Then, PCA and LDA were employed for lessening the dimension of the features. Finally, the extracted feature vectors were classified using ensemble classifier in order to distinguish the healthy and Alzheimer's disease patients. The computational complexity of the developed system was increased by combining more dimensional reduction methods.

J. Samper-Gonzalez et al. [19] used statistical parametric mapping12 and positron emission tomography-partial volume correction software's for image pre-processing. Next, the region and voxel features were extracted from the pre-processed images. In addition, SVM, logistic regression, and random forest were applied to distinguish the normal, MCI, and Alzheimer's disease patients. The experimental result validated that the developed system was only suitable for single modality classification problem. V. Sachnev, and S. Suresh, [20] implemented a diagnosis system for Alzheimer's disease identification based on extreme learning machine (ELM) and sample-balanced genetic algorithms. The ELM algorithm includes a few issues like imbalanced class distribution, and overfitting problem in the medical image applications. S.H. Wang et al. [21] developed a new Alzheimer's disease detection system based on wavelet entropy, multilayer perceptron, and biogeography-based optimization. In this literature, the interclass variation criterion was used for selecting single slice from the three-dimensional volumetric data. The wavelet transform generates same size of coefficients as original three-dimensional brain image that causes a burden to the consequent analysis.

Y. Zhang et al. [22] presented a system for diagnosing Alzheimer's disease automatically from MRI scans. Initially, image processing was accomplished using spatial normalization and skull stripping. Secondly, one axial slice was selected from the volumetric images and then stationary wavelet entropy was used to extract the texture features. Lastly, a single hidden layer neural network was utilized for classifying Alzheimer's disease patients and normal controls [23]. However, single hidden layer neural network was not stable for medical image classification, where it fluctuates among different runs. H. Nawaz et al. [24] developed an Alzheimer's disease detection model based on pre-trained AlexNet. In this literature, deep learning features were extracted from convolutional neural network (CNN). In the experimental phase, the developed model outperformed the machine learning techniques by means of classification accuracy. Hence, the developed model requires a large database for extracting the deep learning features that leads to overfitting and class imbalance concerns [25]. H.S. Suresha, and S.S. Parthasarathy [26] introduced a new automated system for Alzheimer's disease detection. Initially, median filter was applied for denoising the collected images from OASIS dataset. Further, fast-independent component analysis (Fast-ICA) along with Otsu multilevel thresholding was developed for brain tissue segmentation. One of the main issues in Fast-ICA with Otsu multilevel thresholding approach was it includes more outliers that results in misclassification. To address the above-mentioned concerns, a new deep learning system was proposed in the present research for enhancing the performance of Alzheimer's disease detection.

In the present research, the brain images are acquired from two databases such as OASIS and NIMHANS. After the acquisition of brain images, pre-processing is accomplished by normalization and CLAHE techniques. The major benefit of normalization technique is that it brings the range of intensity value to the normal distribution that makes the image looks better for the visualizer. Additionally, CLAHE technique estimates several histograms for redistributing the lightness of the image pixel values, which enhances the color contrast and edges of the brain images. After image denoising, DWT technique is used for extracting the feature vectors from the denoised brain images. DWT technique effectively reveals the local features of the brain images, which helps in the reduction of feature degradation. After feature extraction, PPCA is developed to lessen the dimension of the extracted features. Usually, PPCA uses only a limited number of feature vectors for representing the data that significantly diminish the "curse of dimensionality" issue. Then, the output of PPCA is given as the input for LSTM classifier to classify the brain images as normal, MCI, and Alzheimer's disease. Finally, the performance of the proposed system is compared with the prior systems in terms of false omission rate (FOR), false discovery rate (FDR), sensitivity, error rate, accuracy, and specificity. The simulation results showed that the proposed system obtained 98.78% and 95.88% of classification accuracy on OASIS and NIMHANS datasets.

The graphical illustration of the proposed system is represented in Fig. 1.

Methods

The proposed system majorly contains five phases; brain image datasets, image denoising, transformation, dimensional reduction, and classification. The detailed explanation about each phase is given as follows;

Brain Image Datasets

In this research, OASIS and NIMHANS (real time) datasets are utilized to acquire the brain images. The OASIS dataset comprises of 416 individuals (whose age ranges from 18 to 96). In this research, totally 126 individuals are considered that includes 98 healthy subjects and 28 Alzheimer's disease patients. The statistical information about OASIS dataset is detailed in Table 1. OASIS dataset contains information about the subject's demographics such as number of patients, education, socioeconomic status, age, gender, Mini Mental State Examination (MMSE) score, and Clinical Dementia Rating (CDR). MMSE is a questionnaire test, which is utilized for monitoring the dementia and cognitive impairment. Similarly, CDR is used to measure the severity of dementia on the basis of individual care, community affairs, orientation, residence and hobbies, and memory [27]. The sample images of OASIS dataset are represented in Fig. 2.

Similarly, the NIMHANS dataset comprises of 99 individuals (60 normal controls and 39 Alzheimer's diseases patients), whose age ranges from 55–87 years. In the undertaken dataset, all the individuals are assessed on NNB-E that contains the tests for working memory, visual and verbal spatial memory, executive function, construction, and language [28]. The sample images of NIMHANS dataset are denoted in Fig. 3.

Image Pre-Processing

After collecting the brain images, pre-processing is performed using normalization and CLAHE techniques. Initially, image normalization is applied to alter the image pixel intensity values to improve the quality of acquired brain images by lessening the machinery and impulse noises from the brain images. Then, find the deformations and alternations occurred in the brain images due to imprecise image capture. During image normalization, the acquired brain image is converted into pre-determined

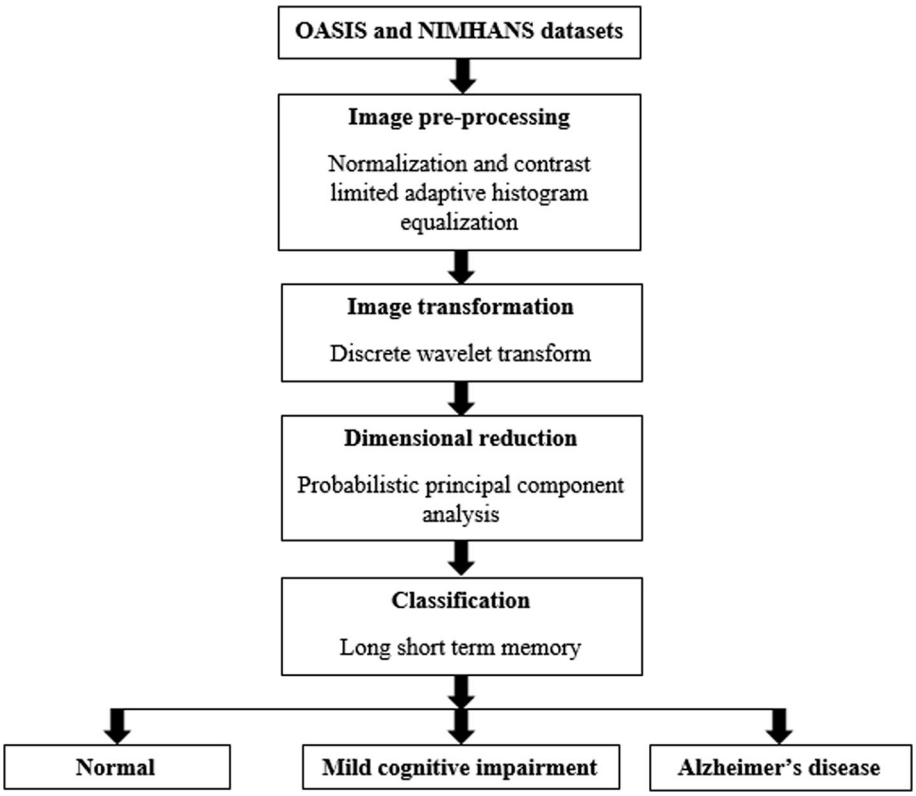

Fig. 1 Flow diagram of the proposed system

Table 1 Description about OASIS dataset

Factor	Alzheimer's diseases	Healthy control
Number of patients	28	98
Education	2.57 ∓ 1.31	3.26 ∓ 1.31
Age (years)	77.75 ∓ 6.99	75.91 ∓ 8.98
MMSE score	21.67 ∓ 3.75	28.95 ∓ 1.20
Socioeconomic status	2.87 ∓ 1.29	2.51 ∓ 1.09
CDR	1	0
Gender (male/female)	9/19	26/72

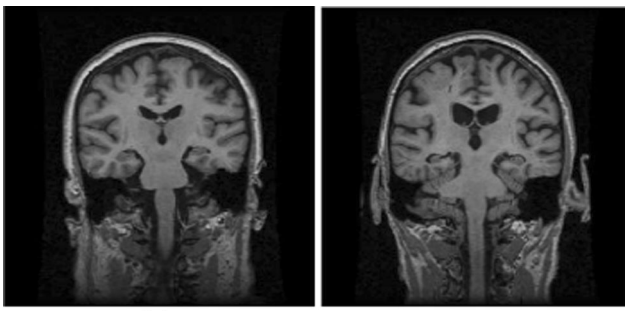

(a) **(b)**

Fig. 3 Sample images of NIMHANS dataset a) normal, and b) MCI

variables [29]. The formula of image normalization is mathematically denoted in Eq. (1).

$$\mathrm{IN} = (1 - M\,\mathrm{min}) + \frac{\text{new Max} - \text{new Min}}{\text{Max} - \text{Min}} + \text{new Min} \tag{1}$$

where I is represented as input brain image, IN is indicated as normalized image, new Max − new Min is stated as intensity range of normalized image, and $\mathrm{Min} = 0$, and $\mathrm{Max} = 255$ is indicated as pixel intensity range of input brain image. The sample normalized brain images of OASIS and NIMHANS datasets are indicated in Figs. 4 and 5.

After image normalization, CLAHE technique is used to further enhance the quality of normalized images in order to achieve the detailed information about the images. The CLAHE technique enhances the local contrast and the definitions of edges in every region of an image. Initially, the normalized brain images are divided into non-overlapping contextual regions, named as sub-images or blocks [30, 31]. Generally, the CLAHE technique consists of two key parameters such as clip limit and block size. Hence, the clip limit is used to smooth the low intensity pixel values and the block size improves the color contrast of the grayscale images. Additionally, the block size and clip limit identify the maximum entropy curvature in order to provide good quality of images using image entropy. Step-by-step process of CLAHE technique is detailed as follows.

At first, the input variables are initialized for image enhancement such as distribution parameter type, number of regions in row and column direction, clip-limit, and dynamic range (no of bins utilized in histogram transfer function).

The normalized brain images are divided into blocks or sub-images and then employ gray level mapping and clipping in the sub-images.

The number of image pixels is equally divided into gray levels in the contextual regions. Therefore, the average number of image pixels is estimated by utilizing Eq. (2).

$$n_{\mathrm{avg}} = \frac{n_{\mathrm{CR}} - y_p \times n_{\mathrm{CR}} - x_p}{n_{\mathrm{grey}}} \tag{2}$$

After estimating the actual clip-limit, Eq. (2) is updated as shown in Eq. (3).

$$n_{CL} = n_{avg} \times n_{CLIP} \tag{3}$$

where n_{avg} is indicated as average number of image pixels, n_{gray} is represented as number of gray levels in the contextual regions, $n_{\mathrm{CR}} - x_p$ and $n_{\mathrm{CR}} - y_p$ are denoted as number of pixels in x and y directions of the contextual regions.

At last, incorporate the gray-level mapping using four pixel clusters, where the resultant image is the enhanced image. The enhanced brain images of OASIS and NIMHANS datasets are specified in Figs. 6 and 7.

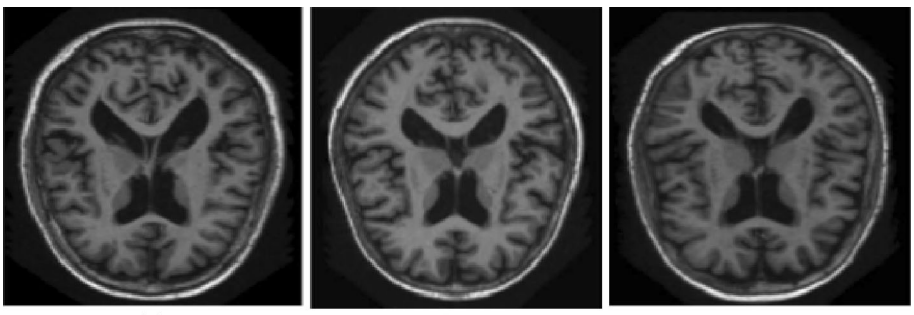

(a) **(b)** **(c)**

Fig. 2 Sample images of OASIS dataset a) normal, b) MCI, and c) Alzheimer's diseases

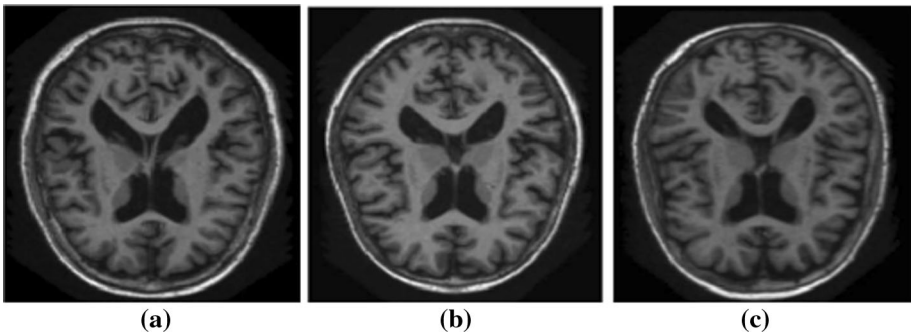

Fig. 4 Sample normalized images of OASIS dataset

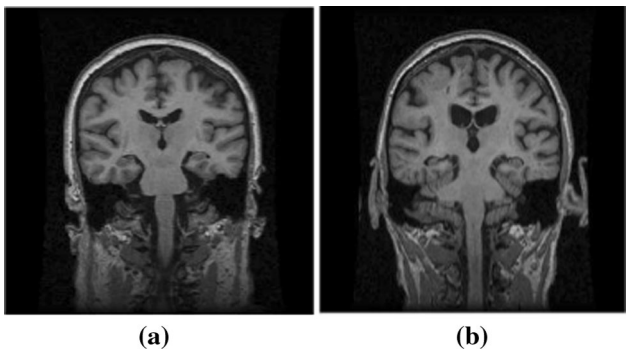

Fig. 5 Sample normalized images of NIMHANS dataset

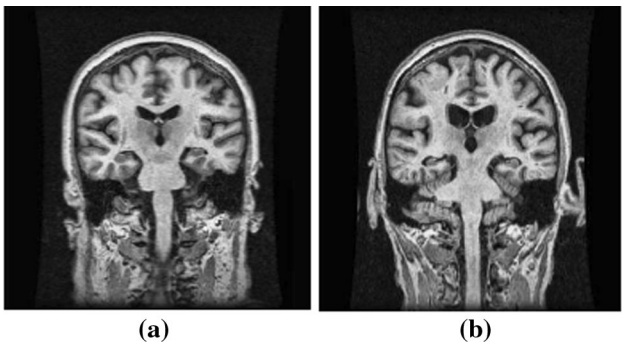

Fig. 7 Enhanced brain images of NIMHANS dataset

Image Transformation

After denoising the brain images, image transformation is accomplished using DWT approach for revealing the local features of the enhanced images that helps in eliminating the irrelevant image features. The two-dimensional DWT approach includes a few advantages like low computation, good energy compression, and low redundancy. The two-dimensional DWT approach is a "rescaled square-shaped function" that generates a wavelet family for separating the low-frequency image components from the high-frequency image components [32]. Initially, transform the brain images into sub-images in different image resolution levels for preserving the both high- and low-level frequency information that assists DWT to extract the useful data from the denoised brain images [33]. The square integral function f(x) and the wavelet transforms are determined as the inner product f and the real valued function R(x) that are mathematically denoted in Eq. (4).

$$w[f(s,\tau)] = \left(f, R^k_{s,t}\right) = \int_{-\infty}^{\infty} f(x) R^k_{s,t}(x)\mathrm{d}x \tag{4}$$

where $R^k_{s,t}(x) = \left(\frac{1}{\sqrt{s}R^k_{s,t}(x-r)} \Big/ s\right)$ is represented as wavelet family, $s \in \tau, z$ and $k \in \{v, h, d\}$ are stated as scale, translation, and orientation parameters. The orientation parameters v, h, and d are indicated as vertical, horizontal, and diagonal directions. In the next segment, the Dyadic wavelet decomposition is undertaken, where $s = 2^j$ and $\tau = 2^j, n, j, n \in z$. Then, the scaling and wavelet families are generated by using the wavelet function R(x), and scaling function $\xi(x)$ that are mathematically denoted in Eqs. (5) and (6).

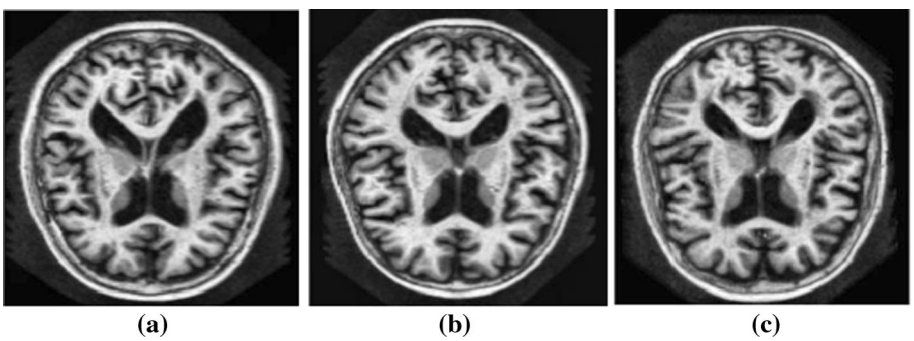

Fig. 6 Enhanced brain images of OASIS dataset

$$R_{j,n}^{k}(x) = \frac{1}{\sqrt{2^j}} R^k\left(\frac{x - 2^j.n}{2^j}\right)$$

$$\xi_{j,n}^{k}(x) = \frac{1}{\sqrt{2^j}} \xi^k\left(\frac{x - 2^j.n}{2^j}\right)$$

Generally, the orthonormal subspaces are related to the resolution 2^j. Henceforth, the wavelet atom is estimated by utilizing the mother atoms R^h, R^v, and R^d, which are determined as tensor product of two-dimensional $\xi(x)$ and $R(x)$ that are stated in Eqs. (7) and (8).

$$\xi(x) = \xi(x_1)\xi(x_2), R^h(x) = R(x_1)R(x_2)$$

$$R^v(x) = \xi(x_1)R(x_2), R^d(x) = R(x_1)\xi(x_2)$$

The two-dimensional DWT technique is executed by utilizing filter banks and down-samplers. Normally, the digital filter bank comprises of high-pass (g) and low-pass (h) filters, and the number of filter bank is assumed as per the resolution in the wavelet configuration. For instance, the enhanced brain image $A_{2^{j+1}}f$ at resolution 2^{j+1} is transformed into four sub-bands in the frequency domain. In the available four sub-bands, three sub-bands are brain images $D_{2^j}^v f, D_{2^j}^d f$ and $D_{2^j}^h f$ at the resolution of 2^j in vertical, diagonal, and horizontal directions. The remaining one sub-band is approximation image $A_{2^j}f$, which is in the coarse resolution format. Though, the entire brain image $A_{2^{j+1}}f$ is mathematically indicated in Eq. (9).

$$A_{2^{j+1}}f = D_{2^j}^h f + D_{2^j}^v f + D_{2^j}^d f + A_{2^j}f \tag{9}$$

The transformed brain images are in the form of two-dimensional orthogonal wavelet.

The wavelet transformation outcome is resultant into four orthogonal sub-bands such as low-high, high-high, low-low, and high-low that corresponds to the sub-images $D_{2^j}^v f, D_{2^j}^d f$ and $D_{2^j}^h f$ and $A_{2^j}f$. A sample wavelet transformed brain image is stated in Fig. 8, and the final result of DWT is represented in Fig. 9.

Feature Dimensional Reduction

After feature extraction, dimensional reduction is performed by applying PPCA [34]. Let us consider $x_i = \left(x_{i1}, \ldots x_{ip}\right)^T$ as the feature vectors, which are extracted from the DWT for the i^{th} subject $i = 1, \ldots n$. The probabilistic representation of PCA is mathematically stated in Eq. (10).

$$x_i = \mu + wu_i + \in_i,\ i = 1, \ldots n$$

where u_i is denoted as principal components, and w is stated as $p \times q$ matrix with elements $w_{\text{jh}}, j = 1, \ldots p, h = 1, \ldots q$. In addition, the term u is

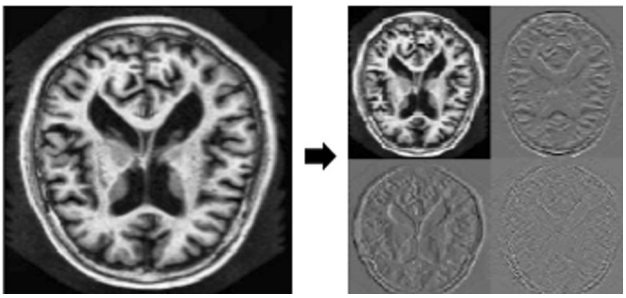

Fig. 8 Sample wavelet transformed brain image

Fig. 9 Final result of DWT

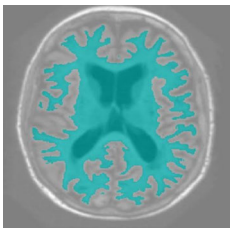

stochastically independent from $\in$, and it is mathematically denoted in Eq. (11).

$$u_i \sim \aleph\left(0, I_q\right)$$

where Iq is indicated as identity matrix of order q. In addition, the error is assumed to be zero-centered Gaussian with covariance matrix $\Psi, \in_i \sim \aleph(0, \Psi)$. Then, the multivariate distribution is obtained by using Eq. (12),

$$x_i \sim \aleph(\mu, C), C = ww^T + \Psi$$

Also, assume $\Psi = \psi I_p, \psi \in \Re_+$, so the elements of x_i are conditionally independent to given u_i. The parameters $\mu = \left(\mu_1, \ldots \mu_p\right)^T$ allow location shift fixed effect, and the marginal log likelihood is mathematically denoted in Eq. (13).

$$l(\theta; X) = -\frac{n}{2}\left\{p\log(2\pi) + \log|C| + tr\left(C^{-1}S\right)\right\}$$

where $S = \left(\frac{1}{n}\right)\sum_{i=1}^{n}(x_i - \mu)(x_i - \mu)^T$ and the parameter $\theta = (\pi, w, \psi)$ are estimated by the maximum likelihood estimation Eqs. (14), (15), and (16).

$$\hat{\mu} = \frac{1}{n}X^T 1_n$$

$$\hat{w} = H_q\left(\Delta_q - \psi I_q\right)^{1/2}\Re \tag{15}$$

$$\hat{\psi} = \frac{1}{p-q}\sum\nolimits_{j=q+1}^{p}\delta_j \tag{16}$$

where $X = (x_i)^T$ is denoted as response matrix, l_n is stated as $n \times 1$ vector, H_q is indicated as principal eigenvectors of the covariance matrix, and $\Re$ is represented as orthogonal rotation matrix. At last, the individual score is predicted by utilizing best linear prediction as shown in Eq. (17).

$$\hat{u} = E(u|x) = \left(w^T w + \Psi\right)^{-1} w^T (x - \mu) \tag{17}$$

Classification

After dimensionality reduction, classification is accomplished by LSTM for classifying the images as normal, MCI, and Alzheimer's disease [35]. Usually, LSTM work based on feature learning that significantly enhances the performance of mapping compared with the manually predicted values. For feature learning, stack auto-encoder is used to analyze the variations in data. In LSTM, the stack auto-encoder contains three layers such as input, hidden, and output layers. Here, the selected feature length is 5×4, which is the size of the input layer. In LSTM, the temporal state, cell of multiplicative gathering unit, and couple of versatile are applied for controlling the data stream in memory block [36, 37].

At first, the consistent error carousels are activated by self-associated direct unit for describing the memory cell state. The multiplicative gateways along with consistent error carousels are used to find the error constant of the system. Then, the forget gate is included in memory block to improve the bound development and to prevent the inner cell values. Restart the memory block, once the consistent error carousel weight replaces the multiplicative forget gateway activation and the data stream is outdated. The LSTM architecture is denoted in Fig. 10.

The input of the model is represented as $x = (x_1, x_2, ...x_T)$, and the output sequence is indicated as $y = (y_1, y_2, \ldots y_T)$, where T is stated as recognition period. Based on prior information, the optimal features are recognized without affecting the previous steps, which is deliberated as a major benefit of LSTM [38]. In order to accomplish this objective, the travel time is iteratively calculated by utilizing Eqs. (18–23).

$$i_t = \Theta(W_{ix}x_t + W_{\Im}m_{t-1} + W_{ic}C_{t-1} + b_i) \tag{18}$$

$$f_t = \Theta\left(W_{fx}Xt + W_{fm}m_{t-1} + W_{fc}C_{t-1} + b_f\right) \tag{19}$$

$$C_t = f_t\Theta C_{t-1} + i_t\Phi g(WcxXt + W_{cm}m_{t-1} + b_c) \tag{20}$$

$$O_t = \Theta(W_{ax}Xt + W_{om}m_{t-1} + W_{oc}C_t + b_o) \tag{21}$$

$$m_t = O_t\Phi h(C_t) \tag{22}$$

$$y_t = W_{ym}m_t + b_y \tag{23}$$

where $\Theta(.)$ is denoted as standard logistic sigmoid function and Φ is represented as vector scalar product. Hence, the sigmoid function $\Theta(.)$ is calculated by applying Eq. (24).

$$\Theta(X) = \frac{1}{1 - e^x} \tag{24}$$

where c_{t,m_t} is signified as activation vectors of every cell and memory blocks, b is indicated as bias vector, and W is indicated as weight matrices. Additionally, $H(.)$ is stated as sigmoid function of centered logistic that ranges from $[-3, 3]$, which is indicated in Eq. (25).

$$H(X) = \frac{4}{1 - e^x} - 3 \tag{25}$$

where $C(.)$ is denoted as sigmoid function of centered logistic that ranges from [2,-2], which is defined in Eq. (26).

$$C(X) = \frac{2}{1 - e^x} - 2 \tag{26}$$

By adjusting the truncated back-propagation and real-time recurrent learning, the LSTM classifier is trained. Before entering into linear consistent error carousel, the truncated errors reached the output of memory cell and the square errors are limited. For time management in LSTM classifier, the self-assertive time slacks are developed with long dependency [39]. The global features are selected utilizing PPCA and it is given as the input to LSTM classifier. In this work, the weight of neural system is controlled by Adam optimizer, because it is productive in computation, easy to implement, invariant to rescaling diagonal gradients, and requires fewer memory space. The parameter setting of LSTM classifier is given as follows; hidden unit is 1000, epoch is 100, and the Mini batch size is 27. In this research study, MATLAB (2018a) software is used for experimental simulation with the system requirements; Intel (R) Core (TM) i5 CPU @ 3.10 GHz and 8 GB (RAM). In this scenario, the proposed system performance is evaluated by means of FOR, FDR, error rate, sensitivity, accuracy, and specificity. The general formula for estimating FOR, FDR, sensitivity, accuracy, error rate, and specificity are indicated in Eqs. (27), (28), (29), (30), (31), and (32).

$$\text{FOR} = \frac{\text{FN}}{\text{TN} + \text{FN}} \times 100 \tag{27}$$

$$\text{FDR} = \frac{\text{FP}}{\text{TP} + \text{FP}} \times 100 \tag{28}$$

$$\text{Sensitivity} = \frac{\text{TP}}{\text{FN} + \text{TP}} \times 100 \tag{29}$$

$$\text{Accuracy} = \frac{\text{TP} + \text{TN}}{\text{TP} + \text{TN} + \text{FP} + \text{FN}} \times 100 \tag{30}$$

$$\text{Error Rate} = 100 - \text{Accuracy} \tag{31}$$

$$\text{Specificity} = \frac{\text{TN}}{\text{FP} + \text{TN}} \times 100 \tag{32}$$

where TP is indicated as true positive, FP is stated as false positive, TN is specified as true negative, and FN is denoted as false negative.

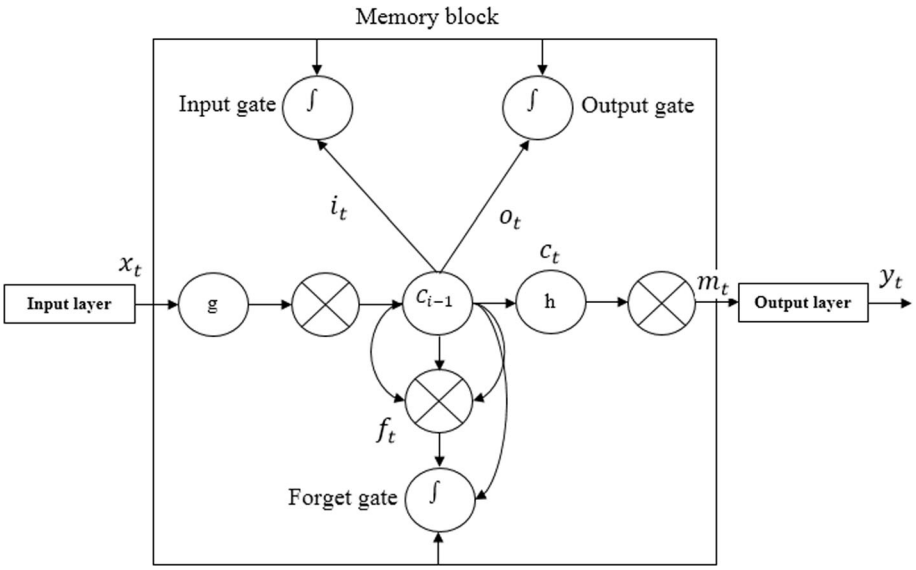

Fig. 10 Architecture of LSTM architecture

Experimental Results

In the experimental result section, the proposed system is compared with a few existing systems (D. Jha et al. [17], D. Jha et al. [18], V. Sachnev, and S. Suresh, [20], S.H. Wang et al. [21], Y. Zhang et al. [22], and H.S. Suresha, and S.S. Parthasarathy [26]) on OASIS database to validate the efficiency of the proposed system. The quantitative and comparative study of the proposed system is given as follows;

Quantitative Study on OASIS Dataset

In this subsection, OASIS dataset is used for analyzing the performance of the proposed system. In Table 2, the performance of the proposed system is assessed by means of specificity, sensitivity, and classification accuracy. Here, the performance valuation is done for 75 images (25 images for normal class, 25 images for MCI class, and the remaining 25 images for Alzheimer's disease class) with 20% testing of images and 80% training of images. In addition, the performance validation is done with dissimilar classification methods such as LSTM, deep neural network (DNN), and convolutional neural network (CNN). From the experimental investigation, the sensitivity of LSTM is 98.43% and the comparative deep learning classification methodologies (DNN and CNN) achieved 93.78% and 90.14% of sensitivity. Similarly, the specificity value of LSTM is 98.01% and the comparative methodologies (DNN and CNN) attained 92.49% and 90.89% of specificity. Furthermore, the accuracy of LSTM methodology is 98.78%, and the available deep learning classifiers (DNN and CNN) achieved 92.29% and 91.48% of accuracy. The graphical comparison of the proposed system by means of accuracy, specificity, and sensitivity on OASIS dataset is denoted in Fig. 11.

In Table 3, the performance of the proposed system is assessed by means of error rate, FOR, and FDR. Correspondingly, the error rate of LSTM approach is 1.22% and the comparative deep learning classification methodologies (DNN and CNN) attained 7.71% and 8.52% of error rate. Likewise, the FOR value of LSTM is 2.12% and the comparative methodologies (DNN and CNN) attained 8.56% and 12.23% of FOR value. In addition, the FDR value of LSTM approach is 1.14% and the undertaken deep learning classifiers (DNN and CNN) achieved 7.97% and 9.12% of FDR value. The graphical comparison of the proposed system in terms of error rate, FOR, and FDR on OASIS dataset is indicated in Fig. 12.

As mentioned above, feature dimensionality reduction and classification are the integral steps in automatic recognition and classification of Alzheimer's disease. After feature extraction, dimensionality reduction is performed to lessen the "curse of dimensionality" issue, where the dimensionally reduced feature vectors are fit for better Alzheimer's disease classification that is shown in Table 4. In this consequence, the performance of the proposed system is validated with dissimilar methods such as LDA, PCA, Independent Component Analysis (ICA), Kernel-PCA (KPCA), and PPCA. The experimental investigation shows that the PPCA algorithm shows higher performance in terms of FOR, FDR, sensitivity, classification accuracy, error rate, and specificity on OASIS dataset. Hence, the PPCA algorithm improved the recognition accuracy up to 2–24% compared with other algorithms in Alzheimer's disease detection and classification.

Table 2 Performance validation by means of accuracy, specificity, and sensitivity on OASIS dataset

Classifier	Sensitivity (%)	Specificity (%)	Accuracy (%)
DNN	93.78	92.49	92.29
CNN	90.14	90.89	91.48
LSTM	98.43	98.01	98.78

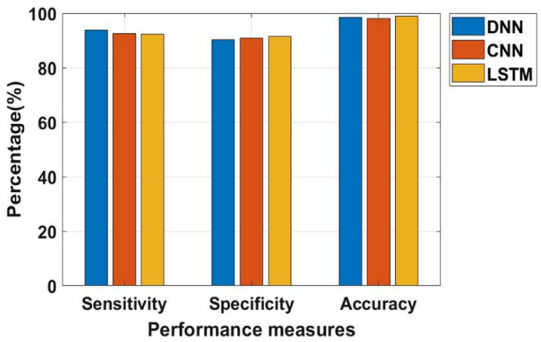

Fig. 11 Graphical comparison of the proposed system in light of accuracy, specificity, and sensitivity on OASIS dataset

Table 3 Performance validation by means of error rate, FOR, and FDR on OASIS dataset

Classifier	Error rate (%)	FOR (%)	FDR (%)
DNN	7.71	8.56	7.97
CNN	8.52	12.23	9.12
LSTM	1.22	2.12	1.14

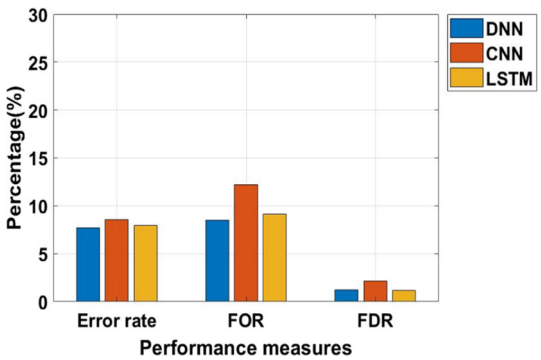

Fig. 12 Graphical comparison of the proposed system in light of error rate, FOR, and FDR on OASIS dataset

Quantitative study on NIMHANS dataset

In this segment, NIMHANS dataset is used to analyze the performance of the proposed system. In Table 5, the proposed system performance is assessed by means of specificity, sensitivity, accuracy, error rate, FOR, and FDR. Here, the performance evaluation is done for 50 images (25 images for normal class, and 25 images for Alzheimer's disease class) with 20% testing and 80% training of the brain images. From the experimental inspection, the recognition accuracy of LSTM is 95.88%, and the existing deep learning classification approaches (DNN and CNN) achieve 87.12% and 90.75%. Correspondingly, the specificity, sensitivity, error rate, FOR, and FDR value of LSTM approach is 94.15%, 93.02%, 4.12%, 6.32%, and 5.79%. Hence, the undertaken classification methodologies (DNN and CNN) achieve minimum sensitivity and specificity, and maximum error rate, FOR, and FDR value compared with LSTM classifier. Graphical comparison of the proposed system by means of sensitivity, accuracy, specificity, error rate, FOR, and FDR on NIMHANS database is represented in Figs. 13 and 14.

In Table 6, the proposed system performance is analyzed with dissimilar dimensionality reduction algorithms on NIMHANS dataset. From the inspection, the recognition accuracy of PPCA is 95.88%, and the existing approaches (ICA, LDA, PCA, and KPCA) achieve 71.35%, 75%, 91.87%, and 85.46% of accuracy. Similarly, the specificity, sensitivity, error rate, FOR, and FDR value of PPCA are superior compared with other approaches. Though, the PPCA includes a few key benefits like effectively dealing with missing values in the dataset, and appropriate for model class conditional densities.

Comparative Study

Table 7 indicates the comparative study of the proposed and the existing systems performance. D. Jha et al. [17] developed a new supervised system for Alzheimer's disease recognition on the basis of PCA, FNN, and DTCWT, where the performance of the developed system was validated on OASIS dataset. The experimental outcome showed that the developed system attained 90.06% of accuracy, and 92% of sensitivity in Alzheimer's disease recognition and classification. In addition, D. Jha et al. [18] presented a new framework for Alzheimer's disease classification based on DTCWT, PCA, LDA, and ensemble classifier. The extensive experiments showed that the developed system achieved 95.72% of accuracy and 96.59% of sensitivity in Alzheimer's disease recognition and classification on OASIS dataset. V. Sachnev, and S. Suresh, [20] presented a diagnosis framework for Alzheimer's diseases identification on the basis of ELM- and sample-balanced genetic algorithm. Extensive experiments were performed on OASIS dataset, and the developed framework attained 87% of recognition accuracy.

S.H. Wang et al. [21] implemented a new Alzheimer's disease detection system on the basis of wavelet entropy, multilayer perceptron, and biogeography-based optimization. Extensive experiments showed that the developed system achieved 92.40% of classification accuracy and

Table 4 Performance valuation of the proposed system with dissimilar dimensionality reduction algorithms on OASIS dataset

Methods	Accuracy (%)	Sensitivity (%)	Specificity (%)	Error rate (%)	FOR (%)	FDR (%)
ICA	74.24	71.05	72.73	25.76	23.29	27.05
LDA	78.19	76.02	77.79	21.81	20.49	25.07
PCA	96.34	96.21	97.35	3.66	3.82	2.92
KPCA	82.97	83.51	81.19	17.03	12.14	13.26
PPCA	98.78	98.01	98.01	1.22	2.12	1.14

Table 5 Performance validation in terms of sensitivity, accuracy, specificity, error rate, FOR, and FDR on NIMHANS dataset

Classifier	Sensitivity (%)	Specificity (%)	Accuracy (%)	Error rate (%)	FOR (%)	FDR (%)
DNN	89.19	88.74	87.12	12.88	15.56	12.19
CNN	89.78	91.57	90.75	9.25	10.35	13.54
LSTM	93.02	94.15	95.88	4.12	6.32	5.79

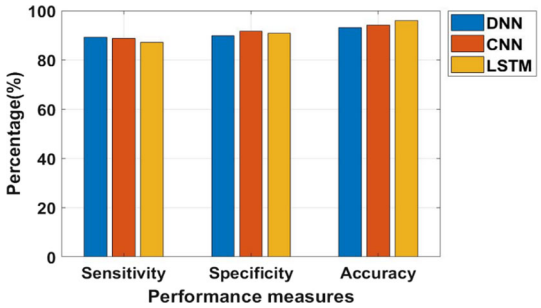

Fig. 13 Graphical comparison of the proposed system by means of accuracy, specificity, and sensitivity on NIMHANS dataset

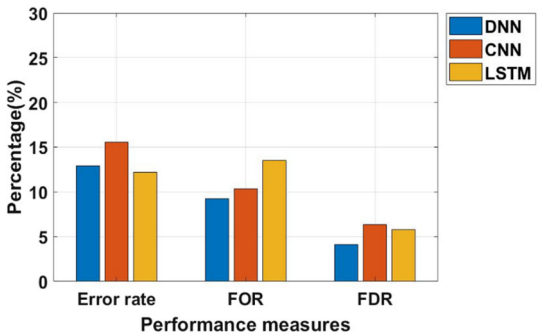

Fig. 14 Graphical comparison of the proposed system by means of error rate, FOR, and FDR on NIMHANS dataset

92.14% of sensitivity on OASIS database. Y. Zhang et al. [22] presented a new machine learning framework to diagnose Alzheimer's diseases from MRI scans. At first, skull stripping and spatial normalization were used for denoising the collected images. Next, stationary wavelet entropy was utilized to extract the texture feature vectors. Finally, single hidden layer neural network with predator prey particle swarm optimization methodology was used to classify the Alzheimer's disease patients and normal controls. Simulation outcome showed that the developed framework achieved 92.73% of classification accuracy, and 92.69% of sensitivity on OASIS database. H.S. Suresha, and S.S. Parthasarathy [26] applied median filter and Fast-ICA with Otsu multilevel thresholding for automated Alzheimer's disease detection. Extensive experiments showed that the developed system obtained 79% of sensitivity on OASIS database. Compared with these existing systems, the proposed system achieved better classification accuracy of 98.78% and sensitivity of 98.01%. In the proposed system, the feature dimensionality reduction is the fundamental part of Alzheimer's disease recognition and classification. Every brain MRI images contain several feature vectors that lead to "curse of dimensionality" issue. So, the feature dimensionality reduction PPCA algorithm plays a crucial role in optimizing the feature vectors, which is appropriate to achieve better disease classification.

Conclusion

An effective deep learning-based supervised system is proposed in this article for the automatic recognition and classification of Alzheimer's disease. The purpose of this work is to classify the brain images as normal, MCI, and Alzheimer's disease by proposing a proper feature dimensional reduction and classification algorithm. In this study, the PPCA algorithm is employed for lessening the dimension of the extracted feature values. The obtained active discriminative feature vectors are classified by applying a deep learning classifier (LSTM). Compared

Table 6 Performance valuation of the proposed system with dissimilar dimensionality reduction algorithms on NIMHANS dataset

Methods	Accuracy (%)	Sensitivity (%)	Specificity (%)	Error rate (%)	FOR (%)	FDR (%)
ICA	71.35	68.72	69.99	28.65	34.59	32.29
LDA	75	73.58	71.46	25	32.41	28.21
PCA	91.87	92.88	92.19	8.13	7.81	8.47
KPCA	85.46	81.54	80.79	14.54	16.39	18.43
PPCA	95.88	93.02	94.15	4.12	6.32	5.79

Table 7 Comparative analysis of proposed and existing systems

Methodology	Accuracy (%)	Senstivity (%)
PCA, FNN, and DTCWT [17]	90.06	92
DTCWT, PCA, LDA, and ensemble classifier [18]	95.72	96.59
ELM- and sample-balanced genetic algorithm [20]	87	-
Wavelet entropy, multilayer perceptron, and biogeography-based optimization [25]	92.40	92.14
Single hidden layer neural network with predator prey particle swarm optimization [26]	92.73	92.69
Fast-ICA with Otsu multilevel thresholding [39]	–	79
Proposed system	98.78	98.01

with the existing systems, the proposed system achieved a better performance in Alzheimer's disease recognition and classification in terms of sensitivity, accuracy, specificity, error rate, FOR, and FDR. From the experimental investigation, the proposed system obtained 98.78% of classification accuracy on OASIS dataset and 95.88% of accuracy on NIMHANS dataset, which are higher compared with the prior systems. In future work, an optimization algorithm is included in the proposed system to improve the performance of Alzheimer's disease recognition and classification. In addition to this, the proposed system is applied to multi-modal data (functional MRI, PET, and MRI) to further improve the accuracy of the brain disease diagnosis.

Funding We haven't received any funding from any sources.

Compliance with Ethical Standards

Conflict of interest Halebeedu Subbaraya Suresha declares that he has no conflict of interest. Srirangapatna Sampathkumaran Parthasarathy declares that he has no conflict of interest.

References

1. C. Zu, B. Jie, M. Liu, S. Chen, D. Shen, D. Zhang, Alzheimer's disease neuroimaging initiative, label-aligned multi-task feature learning for multimodal classification of Alzheimer's disease and mild cognitive impairment. Brain Imaging Behav. **10**, 1148–1159 (2016)
2. R. Mendoza-Léon, J. Puentes, L.F. Uriza, M.H. Hoyos, Single-slice Alzheimer's disease classification and disease regional analysis with Supervised Switching Autoencoders. Comput. Biol. Med. **116**, 103527 (2019)
3. R. Jain, N. Jain, A. Aggarwal, D.J. Hemanth, Convolutional neural network based Alzheimer's disease classification from magnetic resonance brain images. Cognit. Syst. Res. **57**, 147–159 (2019)
4. Y. Qin, Y. Tian, H. Han, L. Liu, X. Ge, H. Xue, T. Wang, L. Zhou, R. Liang, H. Yu, Alzheimer's disease neuroimaging initiative, risk classification for conversion from mild cognitive impairment to Alzheimer's disease in primary care. Psychiatry Res. **278**, 19–26 (2019)
5. T.A. Shaikh, R. Ali, Automated atrophy assessment for Alzheimer's disease diagnosis from brain MRI images. Magn. Reson. Imaging. **62**, 167–173 (2019)
6. K. Hett, V.T. Ta, J.V. Manjón, P. Coupé, Alzheimer's Disease neuroimaging initiative, adaptive fusion of texture-based grading for Alzheimer's disease classification. Comput. Med. Imaging Graph. **70**, 8–16 (2018)
7. M. Liu, J. Zhang, C. Lian, D. Shen, Weakly supervised deep learning for brain disease prognosis using MRI and incomplete clinical scores. IEEE Trans. Cybern. (2019). https://doi.org/10.1109/TCYB.2019.2904186
8. T.M. Schouten, M. Koini, F. De Vos, S. Seiler, M. De Rooij, A. Lechner, R. Schmidt, M. Van den Heuvel, J. Van Der Grond, S.A. Rombouts, Individual classification of Alzheimer's disease with diffusion magnetic resonance imaging. Neuroimage **152**, 476–481 (2017)
9. R.S. Kamathe, K.R. Joshi, A novel method based on independent component analysis for brain MR image tissue classification into CSF WM and GM for atrophy detection in Alzheimer's disease. Biomed Signal Process. Control **40**, 41–48 (2018)
10. I. Beheshti, H. Demirel, H. Matsuda, Alzheimer's Disease neuroimaging initiative, classification of Alzheimer's disease and prediction of mild cognitive impairment-to-Alzheimer's

conversion from structural magnetic resource imaging using feature ranking and a genetic algorithm. Comput. Biol. Med. **83**, 109–119 (2017)
11. T. Ye, C. Zu, B. Jie, D. Shen, D. Zhang, Alzheimer's Disease neuroimaging initiative, discriminative multi-task feature selection for multi-modality classification of Alzheimer's disease. Brain Imaging Behav. **10**, 739–749 (2016)
12. M. Zhang, Y. Yang, F. Shen, H. Zhang, Y. Wang, Multi-view feature selection and classification for Alzheimer's disease diagnosis. Multimed Tools Appl. **76**, 10761–10775 (2017)
13. R. Simoes, A.M.V.C. Van Walsum, C.H. Slump, Classification and localization of early-stage Alzheimer's disease in magnetic resonance images using a patch-based classifier ensemble. Neuroradiology **56**, 709–721 (2014)
14. N. Gao, L.X. Tao, J. Huang, F. Zhang, X. Li, F. O'Sullivan, S.P. Chen, S.J. Tian, G. Mahara, Y.X. Luo, Q. Gao, Contourlet-based hippocampal magnetic resonance imaging texture features for multivariant classification and prediction of Alzheimer's disease. Metab. Brain Dis. **33**, 1899–1909 (2018)
15. D. Baskar, V.S. Jayanthi, A.N. Jayanthi, An efficient classification approach for detection of Alzheimer's disease from biomedical imaging modalities. Multimed. Tools Appl. **78**, 12883–12915 (2019)
16. T. Altaf, S.M. Anwar, N. Gul, M.N. Majeed, M. Majid, Multi-class Alzheimer's disease classification using image and clinical features. Biomed. Signal Process. Control. **43**, 64–74 (2018)
17. D. Jha, J.I. Kim, G.R. Kwon, Diagnosis of Alzheimer's disease using dual-tree complex wavelet transform, PCA, and feed-forward neural network. J. Healthcare Eng. (2017). https://doi.org/10.1155/2017/9060124
18. D. Jha, S. Alam, J.Y. Pyun, K.H. Lee, G.R. Kwon, Alzheimer's disease detection using extreme learning machine, complex dual tree wavelet principal coefficients and linear discriminant analysis. J. Med. Imaging Health Inform. **8**, 881–890 (2018)
19. J. Samper-Gonzalez, N. Burgos, S. Bottani, S. Fontanella, P. Lu, A. Marcoux, A. Routier, J. Guillon, M. Bacci, J. Wen, A. Bertrand, Reproducible evaluation of classification methods in Alzheimer's disease framework and application to MRI and PET data. NeuroImage **183**, 504–521 (2018)
20. V. Sachnev, S. Suresh, An improved sample balanced genetic algorithm and extreme learning machine for accurate Alzheimer disease diagnosis. J. Comput. Sci. Eng. **10**, 118–127 (2016)
21. S.H. Wang, Y. Zhang, Y.J. Li, W.J. Jia, F.Y. Liu, M.M. Yang, Y.D. Zhang, Single slice based detection for Alzheimer's disease via wavelet entropy and multilayer perceptron trained by biogeography-based optimization. Multimed. Tools Appl. **77**(9), 10393–10417 (2018)
22. Y. Zhang, S. Wang, Y. Sui, M. Yang, B. Liu, H. Cheng, J. Sun, W. Jia, P. Phillips, J.M. Gorriz, Multivariate approach for Alzheimer's disease detection using stationary wavelet entropy and predator-prey particle swarm optimization. J. Alzheimers Dis. **65**(3), 855–869 (2018)
23. R.S. Singh, B.S. Saini, R.K. Sunkaria, Arrhythmia detection based on time-frequency features of heart rate variability and back-propagation neural network. Iran J. Comput. Sci. **2**(4), 245–257 (2019)
24. H. Nawaz, M. Maqsood, S. Afzal, F. Aadil, I. Mehmood, S. Rho, A deep feature-based real-time system for Alzheimer disease stage detection". Multimed. Tools Appl. (2020). https://doi.org/10.1007/s11042-020-09087-y
25. I. Kaur, R. Rajni, A. Marwaha, ECG signal analysis and arrhythmia detection using wavelet transform. J. Inst. Eng. India Series B **97**(4), 499–507 (2016)
26. H.S. Suresha, S.S. Parthasarathy, Diagnosis of alzheimer disease using fast independent component analysis and otsu multi-level thresholding. Int. J. Intell. Eng. Syst. **11**(5), 74–83 (2018)
27. D.S. Marcus, T.H. Wang, J. Parker, J.G. Csernansky, J.C. Morris, R.L. Buckner, Open access series of imaging studies (OASIS): cross-sectional MRI data in young, middle aged, nondemented, and demented older adults. J. Cognit. Neurosci. **19**, 1498–1507 (2007)
28. R. Tripathi, J.K. Kumar, S. Bharath, P. Marimuthu, M. Varghese, Clinical validity of NIMHANS neuropsychological battery for elderly: a preliminary report. Indian J. Psychiatry **55**, 279 (2013)
29. K.M. Koo, E.Y. Cha, Image recognition performance enhancements using image normalization. Hum. Centric Comput. Inf. Sci. **7**(1), 1–11 (2017)
30. H. Lidong, Z. Wei, W. Jun, S. Zebin, Combination of contrast limited adaptive histogram equalisation and discrete wavelet transform for image enhancement. IET Image Proc. **9**, 908–915 (2015)
31. J. Ma, X. Fan, S.X. Yang, X. Zhang, X. Zhu, Contrast limited adaptive histogram equalization-based fusion in YIQ and HSI color spaces for underwater image enhancement. Int. J. Pattern Recognit Artif Intell. **32**(07), 1854018 (2018)
32. S. Rekik, N. Ellouze, Enhanced and optimal algorithm for QRS detection. Irbm **38**(1), 56–61 (2017)
33. R. Ashraf, M. Ahmed, S. Jabbar, S. Khalid, A. Ahmad, S. Din, G. Jeon, Content based image retrieval by using color descriptor and discrete wavelet transform. J. Med. Syst. **42**(3), 44 (2018)
34. M. Geraci, A. Farcomeni, Probabilistic principal component analysis to identify profiles of physical activity behaviours in the presence of non-ignorable missing data. J. R. Stat. Soc. Ser. C **65**, 51–75 (2016)
35. K. Priyadarsini, N. Mishra, M. Prasad, V. Gupta, S. Khasim, Detection of malware on the internet of things and its applications depends on long short-term memory network. J. Ambient Intell. Human. Comput. (2021). https://doi.org/10.1007/s12652-020-02823-0
36. F. Chang, T. Chen, W. Su, Q. Alsafasfeh, Control of battery charging based on reinforcement learning and long short-term memory networks. Comput. Electr Eng **85**, 106670 (2020)
37. J. Kang, S. Jang, S. Li, Y.S. Jeong, Y. Sung, Long short-term memory-based malware classification method for information security. Comput. Electr. Eng. **77**, 366–375 (2019)
38. G.J. Jong, C.S. Huang, G.J. Yu, G.J. Horng, Artificial neural network expert system for integrated heart rate variability. Wirel. Pers. Commun. **75**(1), 483–509 (2014)
39. M. Zhou, W. Du, K. Qin, J. Zhou, B. Cai, Distinguish crude and sweated Chinese herbal medicine with support vector machine and random forest methods. Wirel. Pers. Commun. **102**(2), 1827–1838 (2018)